Inorg. Chem. **2002**, *41*, 699–708

Inorganic Chemistry

Article

Oxidative Addition of Phosphine-Tethered Thiols to Iron Carbonyl: Binuclear Phosphinothiolate Complexes, (μ-$SCH_2CH_2PPh_2)_2Fe_2(CO)_4$, and Hydride Derivatives

Xuan Zhao, Yui-May Hsiao, Chia-Huei Lai, Joseph H. Reibenspies, and Marcetta Y. Darensbourg*

Department of Chemistry, Texas A&M University, College Station, Texas 77843

Received July 11, 2001

The mononuclear complex $Fe(CO)_4(PPh_2CH_2CH_2SH)$, **1**, is isolated as an intermediate in the overall reaction of $PPh_2CH_2CH_2SH$ with $[Fe^0(CO)_4]$ sources to produce binuclear bridging thiolate complexes. Photolysis is required for loss of CO and subsequent S–H activation to generate the metal–metal bonded Fe^I–Fe^I complex, (μ-$SCH_2CH_2PPh_2)_2Fe_2(CO)_4$, **2**. Isomeric forms of **2** derive from the apical or basal position of the P-donor ligand in the pseudo square pyramidal $S_2Fe(CO)_2P$ coordination spheres. This position in turn is dictated by the stereochemistry of the μ-S–CH_2 bond, designated as *syn* or *anti* with respect to the Fe_2S_2 butterfly core. Addition of strong acids engages the Fe^I–Fe^I bond density as a bridging hydride, **[(μ-H)-anti-2]**$^+[SO_3CF_3]^-$ or **[(μ-H)-syn-2]**$^+[SO_3CF_3]^-$, with formal oxidation to Fe^{II}–H–Fe^{II}. Molecular structures of **anti-2**, **syn-2**, and **[(μ-H)-anti-2]**$^+[SO_3CF_3]^-$ were determined by X-ray crystallography and show insignificant differences in distance and angle metric parameters, including the Fe–Fe bond distances which average 2.6 Å. The lack of coordination sphere rearrangements is consistent with the ease with which deprotonation occurs, even with the weak base, chloride. The Fe^I–Fe^I bond, supported by bridging thiolates, therefore presents a site where a proton might be taken up and stored as a hydride without impacting the overall structure of the binuclear complex.

Introduction

Thiols are known to oxidatively add to low-valent transition metals, in many cases resulting in aggregation due to the propensity of thiolates to serve as bridging ligands. Thus the addition of PhSH, MeSH, and EtSH to iron(0) carbonyls produces the dinuclear bridging thiolate iron(I) species with release of H_2, eq 1.[1,2]

$$Fe(CO)_5,\ Fe_2(CO)_9,\ \text{or}\ Fe_3(CO)_{12} + RSH \rightarrow [(\mu\text{-SR})Fe(CO)_3]_2 + H_2 + n\text{CO} \quad (1)$$

While this reaction is of obvious importance, and the product is a foundation molecule in organometallic chemistry, the mechanistic pathway of binuclear RS–H oxidative addition has not been mapped. Earlier work demonstrated that the all-CO Fe(0) compound provided no evidence of intermediates in this conversion; however, a monomeric thiolate–hydride $(RS)Fe^{II}$–H intermediate was stabilized by phosphine ligands, Scheme 1.[3,4] In fact, all species shown in Scheme 1 resulting from the protonation of anionic *trans*-$[RSFe(CO)_3(PR_3)]^-$ were indicated in IR and NMR spectroscopic studies. While spectroscopic evidence for the interesting η^2-RSH–Fe interaction was compelling, the complex was nevertheless not isolable.[4] Clearly electron density at iron and the stability of intermediates are fine-tuned by neutral ligand and thiolate donor ability.

An analogue of the thiolate–hydride monomeric intermediate has been prepared by Stephan et al., from the reaction of the phosphine-tethered thiol ligand $PPh_2CH_2CH_2$-SH, P-SH, with Vaska's complex, *trans*-$Ir^I(PPh_3)_2(CO)Cl$.[5] Displacement of a PPh_3 ligand and oxidative addition produced the octahedral Ir(III) hydride complex, Ir^{III}(P-S)(H)$(PPh_3)(CO)Cl$.[5] For the Fe(0) carbonyl reactions such a ligand would tether the bridging thiolate to an $Fe(CO)_2P$ terminus and produce a binuclear complex. Thus, in order to explore the sequence of metal–ligand interaction and S–H

* Author to whom correspondence should be addressed. E-mail: marcetta@mail.chem.tamu.edu.

(1) Hieber, W.; Spacu, P. *Z. Anorg. Allg. Chem.* **1937**, *233*, 353.
(2) King, R. B.; Bisnette, M. B. *Inorg. Chem.* **1965**, *4*, 1663.
(3) Liaw, W.-F.; Kim, C.; Darensbourg, M. Y.; Rheingold, A. L. *J. Am. Chem. Soc.* **1989**, *111*, 3591.
(4) Darensbourg, M. Y.; Liaw, W.-F.; Riordan, C. G. *J. Am. Chem. Soc.* **1989**, *111*, 8051.
(5) Stephan, D. W. *Inorg. Chem.* **1984**, *23*, 2207.

10.1021/ic010741g CCC: $22.00
Published on Web 01/22/2002

Scheme 1

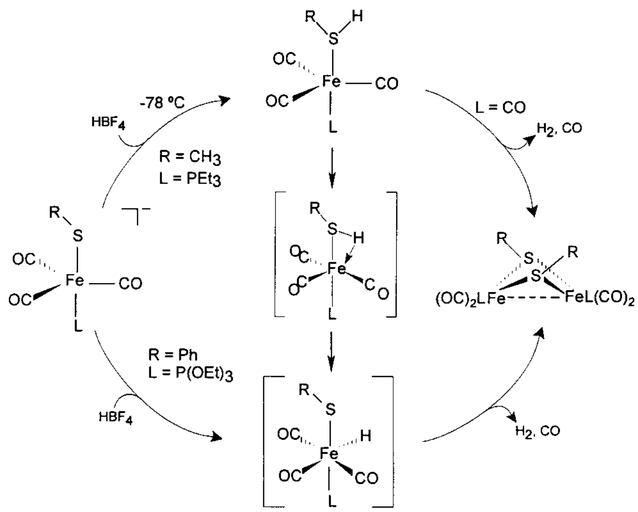

oxidative addition, we have examined the reaction of the P-SH thiol as well as $PMePhCH_2CH_2SH$ and $PMe_2CH_2CH_2$-SH with $[Fe^0(CO)_4]$ sources. In addition, we wished to determine the structures possible for the chelate P-S ligand in binuclear complexes of iron.

Described herein are such products and hydrides derived from protonation of the iron−iron bond in isomeric forms of $(\mu\text{-}SCH_2CH_2PPh_2)_2Fe_2(CO)_4$. Isomerism may result from phosphine position in the pyramidal $Fe(CO)_2PR_3$ units (*trans* or *cis* to the Fe−Fe bond, which is respectively apical or basal in regard to the square pyramidal S_2FeL_3 units),[6] as well as from the orientation of the α-C on the bridging thiolate. Of the possibilities represented below, the *syn* and

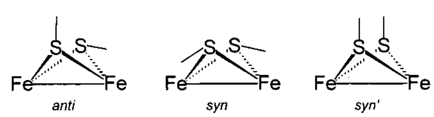

anti forms have been observed for monodentate RS^- bridges[7] and have been shown to exact important steric effects in PR_3/CO exchange reactions.[8,9] The *syn′* form has been observed only in bidentate dithiolate bridges, as in ethanedithiolatediironhexacarbonyl, $(\mu\text{-}SCH_2CH_2S)Fe_2(CO)_6$,[10] or the propanedithiolate analogue, $(\mu\text{-pdt})Fe_2(CO)_6$.[11] The latter and its dicyano derivative prepared from CN^-/CO exchange have found use as structural and spectroscopic models of the dinuclear active site of Fe-only hydrogenase.[12−14]

(6) De Beer, J. A.; Haines, R. J.; Greatrex, R.; Greenwood, N. N. *J. Chem. Soc. A* **1971**, 3271.
(7) Borgne, G. L.; Grandjean, D. *J. Organomet. Chem.* **1977**, *131*, 429.
(8) Maresca, L.; Greggio, F.; Sbrignadello, G.; Bor, G. *Inorg. Chim. Acta* **1972**, *5*, 667.
(9) De Beer, J. A.; Haines, R. J.; Greatrex, R.; Greenwood, N. N. *J. Organomet. Chem.* **1971**, *27*, C33.
(10) Messelhaeuser, J.; Lorenz, I. P.; Haug, K.; Hiller, W. *Z. Naturforsch, B: Anorg. Chem., Org. Chem.* **1985**, *40B*, 1064.
(11) Lyon, E. J.; Georgakaki, I. P.; Reibenspies, J. H.; Darensbourg, M. Y. *Angew. Chem., Int. Ed.* **1999**, *38*, 3178.
(12) Schmidt, M.; Contakes, S. M.; Rauchfuss, T. B. *J. Am. Chem. Soc.* **1999**, *121*, 9736.
(13) Lyon, E. J.; Georgakaki, I. P.; Reibenspies, J. H.; Darensbourg, M. Y. *J. Am. Chem. Soc.* **2001**, *123*, 3268.
(14) Nicolet, Y.; Lemon, B. J.; Fontecilla-Camps, J. C.; Peters, J. W. *Trends Biochem. Sci.* **2000**, *25*, 138.

Experimental Section

Materials and Methods. All manipulations were performed using standard Schlenk techniques under Ar or in an argon atmosphere glovebox. Solvents were reagent grade and purified as follows: Dichloromethane was distilled over phosphorus pentoxide under N_2, and acetonitrile was distilled once from CaH_2 and once from P_2O_5 and freshly distilled from CaH_2 immediately before use. Tetrahydrofuran, diethyl ether, and hexane were distilled from sodium benzophenone ketyl under N_2. The following materials were of reagent grade and used as received: diiron nonacarbonyl, iron pentacarbonyl, trimethylamine *N*-oxide dihydrate, methylphenylphosphine, and trifluoromethanesulfonic acid (Aldrich Chemical Co.), and deuterated solvents (Cambridge Isotope Laboratories).

Instrumentation. Infrared spectra were recorded on a Mattson Galaxy 6021 or an IBM IR/32 using 0.1 mm NaCl cells or KBr pellets. ^1H and ^{31}P NMR spectra were obtained on XL200E Varian and a Unity+ 300 MHz superconducting NMR spectrometers. Cyclic voltammograms were recorded on a BAS-100A electrochemical analyzer using $AgNO_3$ as reference electrode, Pt as counter electrode, and a glassy carbon working electrode with 0.1 M $[n\text{-}Bu_4N][PF_6]$ as electrolyte. All potentials were scaled to NHE using ferrocene as an internal standard.[15] Photochemical reactions were performed in water-jacketed cells using a 450 W mercury lamp. Elemental analyses were performed by Galbraith Laboratories, Inc., Knoxville, TN.

Syntheses. The ligand $PPh_2CH_2CH_2SH$ was prepared as described in the literature,[16] and a similar approach yielded $PPhMeCH_2$-CH_2SH. For the latter, 7.5 g (0.06 mol) PPhMe(H) was dissolved in 70 mL of THF, to which 6 mL of 10 M *n*-BuLi was added dropwise over 15 min with stirring, forming an orange solution. After 30 min, 3.6 mL (0.06 mol) of ethylene sulfide in 125 mL of THF was added dropwise over 1 h; the solution gradually changed to light yellow. After stirring for another hour, 10 mL of a saturated aqueous NH_4Cl solution was added and stirred for 10 min. The organic layer was separated and dried over Na_2SO_4. Distillation under reduced pressure (130 °C/0.5 Torr) gave the product as a colorless liquid (9.3 g, 84%).

The $PMe_2CH_2CH_2SH$ ligand preparation was modified slightly from the literature report.[17] Sodium metal (1.49 g or 65 mmol) was placed in a 250 mL three-neck flask into which 100 mL of liquid ammonia was condensed at dry ice/acetone bath temperature. To the blue solution, 3.94 g (32 mmol) of tetramethyldiphosphane was added dropwise. Over the course of 1 h, the stirred solution changed to yellow, following which time a cooled (dry ice/acetone) portion (3.8 mL, 64 mmol) of ethylene sulfide was transferred into it, stirring being maintained for 1−2 h. The cooling bath was removed to evaporate NH_3; then 20 mL of saturated aqueous NH_4Cl solution was added slowly and stirred for 20 min. The organic layer was separated and dried over Na_2SO_4. Distillation under reduced pressure (70°/0.5 Torr) gave a colorless liquid (2.5 g, 32% yield).

Preparation of $Fe(CO)_4(PPh_2CH_2CH_2SH)$ (1): Method A. Fe_2-$(CO)_9$ (1.0 g, 2.74 mmol) was placed in a 500 mL Schlenk flask with $PPh_2CH_2CH_2SH$ (0.7 g, 2.85 mmol). A total of 200 mL of THF was added to give a brown solution. The reaction mixture was stirred overnight, leading to a reddish brown solution, after which time the solvent was removed under vacuum. This residue was washed with 15 mL of hexane and dried under vacuum to

(15) Gagne, R. R.; Koval, C. A.; Lisensky, G. C. *Inorg. Chem.* **1980**, *19*, 2854.
(16) Chatt, J.; Dilworth, J. R.; Schmutz, J. A. *J. Chem. Soc., Dalton Trans.* **1979**, 1595.
(17) Kita, M.; Yamamoto, T.; Kashiwabara, K.; Fujita, J. *Bull. Chem. Soc. Jpn.* **1992**, *65*, 2272.

Table 1. Infrared Data in Carbonyl Stretching Frequency Region of the Fe_2S_2 Derivatives

compound	ν(CO), cm^{-1}
$Fe(CO)_4(PPh_2CH_2CH_2SH)$, **1**	2053 (m), 1981 (m), 1948 (s), 1941 (s)[a]
$Fe(CO)_4(PPhMeCH_2CH_2SH)$, **1a**	2047 (s), 2008 (m), 1985 (m), 1935 (s)[a]
$Fe(CO)_4(PMe_2CH_2CH_2SH)$, **1b**	2047 (ms), 1968 (ms), 1933 (s,b)[b]
syn-(μ-$SCH_2CH_2PPh_2)_2Fe_2(CO)_4$, **syn-2**	1985 (m), 1960 (s), 1910 (s), 1903 (sh)[b]
anti-(μ-$SCH_2CH_2PPh_2)_2Fe_2(CO)_4$, **anti-2**	1981 (w), 1960 (s), 1912 (s), 1904 (sh)[b]
(μ-$SCH_2CH_2PPh_2)_2Fe_2(CO)_4^-$, **3**	1959 (s), 1897 (s,br) 1732 (m)[c]
(μ-$SCH_2CH_2PPh_2)_2Fe_2(CO)_4^{2-}$, **4**	1959 (s), 1897 (s), 1732 (m)[c]
[(μ-H)-anti-2]$^+(SO_3CF_3)^-$	2053 (m), 2033 (s), 2000 (m, br)[b]
[(μ-H)-syn-2]$^+(SO_3CF_3)^-$	2049 (sh), 2039 (s), 1995 (m, br)[b]

[a] *n*-Hexane solution. [b] THF solutions. [c] Recorded as Na^+ salts in CH_3CN solution.

give a red brown solid (0.60 g, 53% yield). Infrared data in the ν(CO) region is given in Table 1. Elemental anal. Calcd (found) for $C_{18}H_{15}PSO_4Fe$: C, 52.2 (51.8); H, 3.65 (3.60).

Method B. The procedure is the same as in method A using $Fe_3(CO)_{12}$ (1.0 g, 2 mmol) as iron source and $PPh_2CH_2CH_2SH$ (0.7 g, 2.85 mmol).

Method C. At −30 °C, $Me_3NO\cdot 2H_2O$ (113 mg, 1.02 mmol) in methanol was slowly added to $Fe(CO)_5$ (0.14 mL, 1.02 mmol) in THF to give a pale pink solution. To this solution was added 20 mL of a THF solution of $PPh_2CH_2CH_2SH$ (250 mg, 1.02 mmol) to give a reddish solution. The reaction mixture was allowed to warm to room temperature and stirred for 2 h, after which time the solvent was removed under vacuum. The residue was redissolved in THF and filtered through Celite filter, and the filtrate was evaporated to dryness under vacuum. Trituration of the solid in 40 mL of hexane under N_2 was followed by removal of the hexane by cannula. The product was dried in a vacuum to give a red brown solid (295 mg, 70% yield).

Synthesis of $Fe(CO)_4[P(CH_3)_2CH_2CH_2SH]$ and $Fe(CO)_4[PPh(CH_3)CH_2CH_2SH]$. According to method A above, 0.54 g (4.4 mmol) of $P(CH_3)_2CH_2CH_2SH$ and 1.62 g (4.4 mmol) of $Fe_2(CO)_9$ were placed in a 100 mL Schlenk flask, 20 mL of THF was added, and the mixture was stirred for 4 h; a red brown solution was formed. The solvent was removed under reduced pressure; the residue was washed with hexane and dried under vacuum. Yield: 0.60 g (47%). A brown solid in similar yield was obtained from reaction of the $PPh(CH_3)CH_2CH_2SH$ ligand with $Fe_2(CO)_9$ following the same procedure. Infrared data are given in Table 1.

Preparation of (μ-$SCH_2CH_2PPh_2)_2Fe_2(CO)_4$, 2. $Fe(CO)_4(PPh_2CH_2CH_2SH)$ (1.00 g, 2.42 mmol) in 150 mL of THF was irradiated at 22 °C in a photochemical reaction vessel with a water-jacketed 450 W mercury lamp while the solution was gently purged with argon in order to remove liberated carbon monoxide. Irradiation was continued for about 2 h, resulting in complete $Fe(CO)_4(PPh_2CH_2CH_2SH)$ disappearance as indicated by IR. Under Ar, the solution was transferred to a Schlenk flask and the solvent removed under vacuum. This red brown residue was washed with 3 × 10 mL portions of hexane and dried in vacuo. This residue was extracted with 50 mL of ether, producing a red ether solution and leaving a red solid. On vacuum removal of solvent from the ether extract, 75 mg of a red-brown solid was recovered. The product was identified as *syn*-(μ-$SCH_2CH_2PPh_2)_2Fe_2(CO)_4$ **(syn-2)**, by X-ray crystallography (vide infra) and infrared spectroscopy, Table 1. Elemental anal. Calcd (found) for *syn*-(μ-$SCH_2CH_2PPh_2)_2Fe_2(CO)_4$, $C_{32}H_{28}P_2S_2O_4Fe_2$: C, 53.8 (53.3); H, 3.92 (4.18).

The ether insoluble portion from the above reaction was dissolved in 1 mL of THF, after which 15 mL of hexane was added to precipitate a red brown solid. Upon removal of the mother liquor and drying under vacuum, *anti*-(μ-$SCH_2CH_2PPh_2)_2Fe_2(CO)_4$ **(anti-2)** was obtained in 35% yield. See Table 1 for IR data. Elemental anal. Calcd (found) for **anti-2**, $C_{32}H_{28}P_2S_2O_4Fe_2$: C, 53.8 (53.9); H, 3.92 (4.10). X-ray quality crystals of both the *syn* and anti isomers were obtained by hexane diffusion into THF and CH_2Cl_2 solutions, respectively.

Preparation of (μ-$SCH_2CH_2PPhMe)_2Fe_2(CO)_4$. Photochemical irradiation of 0.50 g (1.4 mmol) of $[PPh(CH_3)CH_2CH_2SH]Fe(CO)_4$ dissolved in 100 mL of THF required 2−3 h to reach complete conversion to dimeric (μ-$SCH_2CH_2PPhMe)_2Fe_2(CO)_4$. Following vacuum removal of solvent the product was extracted into 50 mL of diethyl ether. Removal of ether left a red-brown solid (0.20 g, 48% yield). The ν(CO) IR data is given in Table 1. Elemental anal. Calcd (found) for $C_{22}H_{24}P_2S_2O_4Fe_2$: C, 44.8 (45.0); H, 4.10 (4.30).

Protonation of *anti*-(μ-$SCH_2CH_2PPh_2)_2Fe_2(CO)_4$, anti-2. At room temperature, an excess of CF_3SO_3H (0.1 mL, 1 mmol) was added to a solution of **anti-2** (360 mg, 0.5 mmol) in 60 mL of THF under argon. The color of the solution gradually changed from dark red to orange-red. After stirring for 2 h, the solvent was removed, giving a red oil. This residue was washed with 3 × 10 mL of diethyl ether or until the diethyl ether solution was colorless. The product was then extracted into THF (∼50 mL) and filtered through Celite. The solvent volume was reduced to 3 mL, and addition of ∼40 mL of diethyl ether gave an orange-red solid (300 mg, 65% yield). ^1H NMR (d_6-acetone): −16.9 (d of d, 1 H, Fe−H), 1.25−3.42 (m, 8 H, PCH_2CH_2S), 6.90−8.10 (m, 20 H, C_6H_5). Elemental anal. Calcd (found) for $C_{33}H_{29}P_2S_3O_7F_3Fe_2$: C, 45.8 (45.7); H, 3.38 (3.28).

Protonation of *syn*-(μ-$SCH_2CH_2PPh_2)_2Fe_2(CO)_4$, syn-2. The procedure is the same as described for **anti-2**. A red solid was obtained in 65% yield. IR (THF, cm^{-1}): ν(CO) 2052 (sh), 2039 (s), 1995 (m, br). ^1H NMR (d_6-acetone): −17.4 (t, 1 H, Fe−H), 1.58−3.41 (m, 8 H, PCH_2CH_2S), 7.20−8.20 (m, 20 H, C_6H_5). Elemental anal. Calcd (found) for $C_{33}H_{29}P_2S_3O_7F_3Fe_2$: C, 45.8 (45.3); H, 3.38 (3.44).

Deprotonation of {(μ-H)(μ-$SCH_2CH_2PPh_2)_2Fe_2(CO)_4$}$^+$($SO_3CF_3)^-$. Typically, weighed samples of the hydride were placed into a Schlenk flask inside an argon-filled glovebox. After the stoppered flask was transported outside the box, THF or CH_3CN solvents were added, followed by the deprotonation agents Et_3N, and NEt_4CN or PPNCl, dissolved in CH_3CN. The reactions were monitored by IR or NMR techniques. For example, to a 15 mL THF solution of the **[(μ-H)-anti-2]**$^+[SO_3CF_3]^-$ (170 mg, 0.20 mmol) was added Et_3N (0.28 mL, 2 mmol). The orange-red solution turned dark red immediately. New ν(CO) peaks were observed in the IR at 1989 (m, s), 1952 (s), 1921 (m), and 1904 (m) cm^{-1}. This product showed no upfield hydride resonance in the ^1H NMR.

With identical quantities as above, 10 equiv of Et_3N (0.28 mL, 2 mmol) and **[(μ-H)-syn-2]**$^+[SO_3CF_3]^-$ (170 mg, 0.2 mmol) in 15 mL of THF were stirred at room temperature, requiring overnight to produce the final product. The slow reaction produced a dark red solution which exhibited ν(CO) bands at 1984 (w), 1960 (s), and 1912 (s) cm^{-1}. The triplet resonance at −17.3 ppm in the ^1H NMR spectrum of **[(μ-H)-syn-2]**$^+[SO_3CF_3]^-$ disappeared.

Reduction of (μ-$SCH_2CH_2PPh_2)_2Fe_2(CO)_4$. Under argon, a solution of (μ-$SCH_2CH_2PPh_2)_2Fe_2(CO)_4$ (200 mg, 0.28 mmol) as a mixture of isomers in 60 mL of CH_3CN was transferred to a flask containing Na/Hg amalgam (13 mg Na, 0.57 mmol, in 0.6 mL of Hg). The mixture was magnetically stirred for 2 h or until change in the IR to ν(CO) = 1959 (s), 1897 (s, br), 1732 (m) was complete. This solution was anaerobically filtered through Celite into a flask containing solid PPNCl (160 mg, 0.28 mmol). After being stirred at ambient temperature for 1 h, the solution was concentrated to

Scheme 2

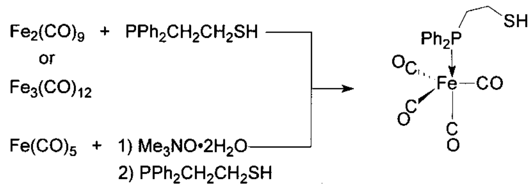

10 mL. Diethyl ether was then slowly added to give a red brown solid (210 mg, 60% yield). IR (CH_3CN, cm^{-1}): ν(CO) 1959 (s), 1897 (s), 1732 (m).

Reduction of $[(\mu\text{-H})\text{-}2]^+[SO_3CF_3]^-$. To a solution of 0.173 g (0.2 mmol) of $[(\mu\text{-H})\text{-}2]^+[SO_3CF_3]^-$ as a mixture of isomers dissolved in 15 mL of CH_3CN was added 0.113 g (0.6 mmol) of Cp_2Co in 10 mL of CH_3CN. The orange red solution turned to red brown gradually. After stirring overnight the resulting red brown solution showed three ν(CO) bands at 1910, 1956, and 1986 cm^{-1}, similar in position and pattern to those of **2**.

X-ray Structure Determination. The X-ray crystal structures were solved at the Crystal & Molecular Structure Laboratory Center at Texas A&M University. X-ray crystallographic data were obtained on a Nicolet R3m/V X-ray diffractometer with an oriented graphite monochromator or a Siemens R3m/V single-crystal X-ray diffractometer operating at 55 kV and 30 mA, M*o* Kα (λ = 0.71073 Å) radiation equipped with a Siemens LT-2 cryostat. All crystallographic calculations were performed with use of the Siemens SHELXTL-PLUS program package.[18] The structures were solved by direct methods. Anisotropic refinement for all non-hydrogen atoms was done by a full-matrix least-squares method. The hydride was located in a difference Fourier map and was refined. Cell parameter and collection data along with atomic coordinates and equivalent isotropic displacement parameters are provided in the Supporting Information.

Results

Syntheses of $Fe(CO)_4(PPh_2CH_2CH_2SH)$, Anti and Syn Forms of $(\mu\text{-}SCH_2CH_2PPh_2)_2Fe_2(CO)_4$, and Conjugate Acids. Reaction of $PPh_2CH_2CH_2SH$ with iron carbonyl sources $Fe_2(CO)_9$ or $Fe_3(CO)_{12}$ in THF at ambient temperature for several hours leads to a red brown solution containing a carbonyl derivative which, on the basis of ν(CO) IR spectroscopy and subsequent derivative chemistry, was identified as $Fe(CO)_4(PPh_2CH_2CH_2SH)$ (**1**), Scheme 2. This complex can also be prepared by decarbonylation of $Fe(CO)_5$ with $Me_3NO{\bullet}2H_2O$ in methanol,[19] followed by reaction with 1 equiv of $PPh_2CH_2CH_2SH$, as indicated in Scheme 2. The IR spectrum of **1**, Figure 1a, has CO stretching frequencies similar to those of the monosubstituted $Fe(CO)_4PR_3$.[20] The two lowest energy bands in the hexane solution ν(CO) IR spectrum, at 1948 (s) and 1941 (s) cm^{-1}, are assigned as an E band, split under pseudo C_{3v} symmetry as imposed by the asymmetrical PPh_2R ligand at the axial position of trigonal bipyramidal $LFe(CO)_4$. The resolution of the E vibrational mode into two bands is not seen in THF. Similar ν(CO) IR spectral patterns were observed for products of the reaction of $Fe_2(CO)_9$ with the ligands $PPhMeCH_2CH_2SH$, **1a**, and $PMe_2CH_2CH_2SH$, **1b**. While the trend noted in Table 1 is to lower ν(CO) position with increasing number of methyl groups, the shift is minimal, despite the concomitant increasing electron donor character of the phosphines. This observation is consistent with simpler $Fe(CO)_4(PR_3)$ complexes and bespeaks the complicated interplay of ν(CO) values, stretching force constants, and electron density at iron.[20]

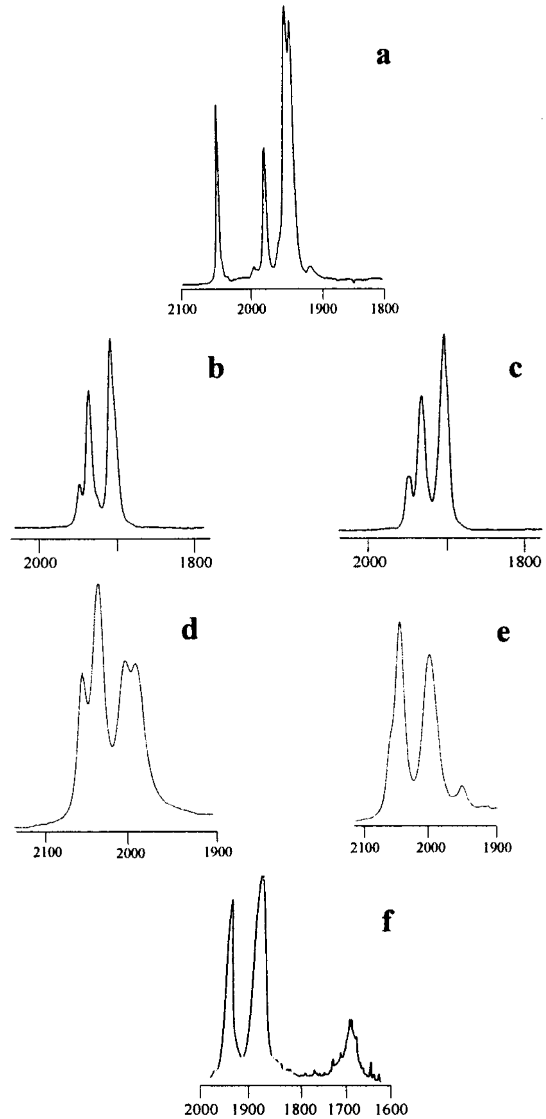

Figure 1. Solution infrared spectra of (a) $Fe(CO)_4(PPh_2CH_2CH_2SH)$ in hexane; (b) *anti*-$(\mu\text{-}SCH_2CH_2PPh_2)_2Fe_2(CO)_4$ in THF; (c) *syn*-$(\mu\text{-}SCH_2CH_2PPh_2)_2Fe_2(CO)_4$ in THF; (d) *anti*-$[(\mu\text{-H})(\mu\text{-}SCH_2CH_2PPh_2)_2Fe_2(CO)_4]^+[CF_3SO_3]^-$ in CH_3CN; (e) *syn*-$[(\mu\text{-H})(\mu\text{-}SCH_2CH_2PPh_2)_2Fe_2(CO)_4]^+[CF_3SO_3]^-$ in CH_3CN; and (f) product from reduction of $(\mu\text{-}SCH_2CH_2PPh_2)_2Fe_2(CO)_4$ by Na/Hg for 1 h at room temperature, in CH_3CN.

Complex **1** is stable in solution at room temperature as well as elevated temperatures (refluxing THF) for extended periods. Nevertheless, photochemical irradiation of a THF solution of $Fe(CO)_4(PPh_2CH_2CH_2SH)$ at room temperature for 1−2 h (depending on the efficacy of the photochemical lamp) resulted in compound **2**, $(\mu\text{-}SCH_2CH_2PPh_2)_2Fe_2(CO)_4$,

(18) (a) Sheldrick, G. *SHELXTL-86 Program for Crystal Structure Solution*; Institut für Anorganische Chemie der Universität: Tammanstrasse 4, D-3400 Göttingen, Germany, 1986. (b) Sheldrick, G. *SHELXTL-93 Program for Crystal Structure Solution*; Institut für Anorganische Chemie der Universität: Tammanstrasse 4, D-3400 Göttingen, Germany, 1993.
(19) Shvo, Y.; Hazum, E. *J. Chem. Soc., Chem. Commun.* **1975**, 829.
(20) Conder, H. L.; Darensbourg, M. Y. *J. Organomet. Chem.* **1974**, *67*, 93.

Scheme 3

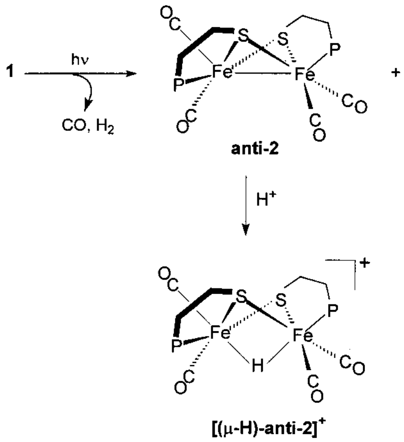

as a mixture of isomers, separable by differences in solubilities and measured to be in anti:syn ratios ranging from 4:1 to 6:1. The gases released during this reaction were verified by gas chromatography to be H_2 and CO. The stick drawings in Scheme 3 are based on the molecular structures as determined by X-ray crystallography, vide infra.

The anti and syn isomers of (μ-$SCH_2CH_2PPh_2$)$_2Fe_2(CO)_4$, so named as described above, showed almost identical infrared spectra in the CO stretching frequency range, differing only in relative intensities (Table 1 and Figure 1). This observation was consistent with the ν(CO) IR spectra of the anti and syn forms of [(μ-SR)$Fe(CO)_3$]$_2$ (R = C_6F_5, C_6Cl_5, CH_3)[8] and [(μ-SPh)$Fe(CO)_2P(OR)_3$]$_2$ (R = CH_3, C_2H_5, C_3H_7).[21]

As indicated in Scheme 3, **anti-2** and **syn-2** reacted with a slight excess of CF_3SO_3H in THF solution, yielding orange red solutions from which air-stable orange solids were obtained on removal of solvent. Spectral properties are presented below. The **[(μ-H)-anti-2]$^+$**[SO_3CF_3]$^-$ crystallized from CH_3CN/Et_2O in suitable crystallinity for X-ray crystal structure analysis.

Molecular Structures of anti-2, syn-2, and [(μ-H)-anti-2]$^+$[SO_3CF_3]$^-$. X-ray crystallographic data are listed in the Supporting Information. Molecular structures are presented in Figures 2−4, and selected bond distances and angles for **anti-2** and **[(μ-H)-anti-2]$^+$** are found in Table 2. Analogous data for **syn-2** are given in Table 3.

The coordination spheres of iron in both binuclear neutral complexes contain two CO, two S from bridging thiolates, and one phosphine, in a distorted square pyramidal arrangement. The pair of electrons in the metal−metal bond orbital overlap resides *trans* to the apical position of the square pyramid and fulfills an octahedral electronic distribution. Nevertheless, the displacement of the iron atom from the best basal planes toward the apical position of 0.25 and 0.42 Å (respectively for Fe(1) and Fe(2) in **anti-2**), and 0.33 and 0.28 Å (respectively for Fe(1) and Fe(2) in **syn-2**) is fully consistent with known square pyramidal geometries and indicates a modest structural requirement of the metal−metal bond density. While the bridging hydride of **[(μ-H)-anti-2]$^+$** renders the irons six-coordinate, there is still a displacement of the iron atoms toward the "apical" ligands, i.e., those *trans* to the μ-H, of 0.12 (Fe(1)) and 0.24 Å (Fe(2)). These displacements are also affirmed by the $\angle L_{apical}-Fe-L_{basal}$ of >90°, ranging from 92.1° to 107.6°. An exception is the $\angle$P(1)−Fe(1)−S(1) angles in **anti-2** and **[(μ-H)-anti-2]$^+$**, which at 88.4° and 87.2°, respectively, represent the restriction of the P-S chelate bite angle and is maintained in all structures.

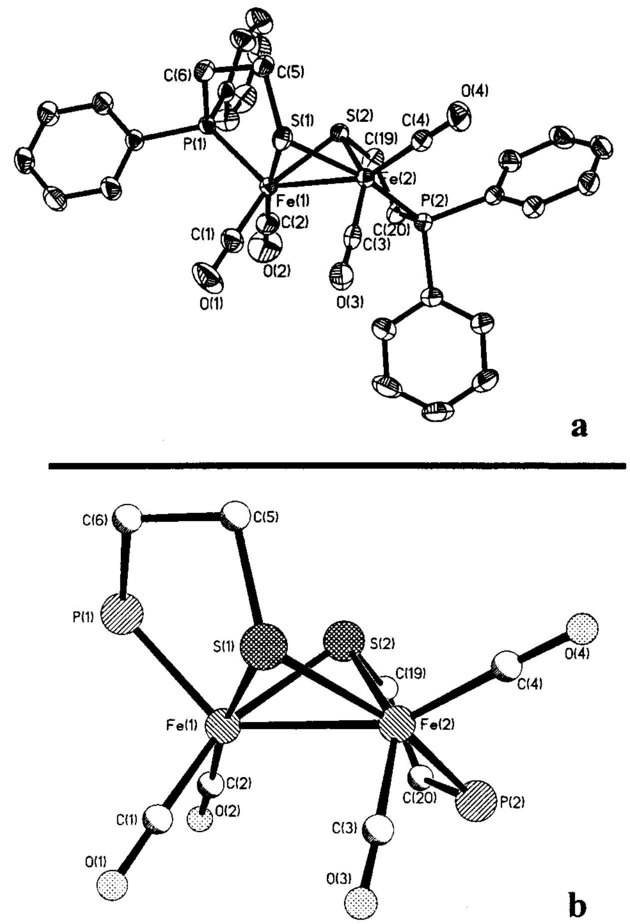

Figure 2. (a) Thermal ellipsoid (50%) and (b) ball-and-stick representations of the molecular structure of **anti-2**.

The orientation of the α-C on the bridging thiolates dictates the position of phosphorus atoms on each iron. For **anti-2**, P(1) atom of the P-S ligand at the Fe(1) center is *trans* to the metal−metal bond (in the apical position of the pseudo square pyramid), while the P(2) atom attached on Fe(2) is *trans* to the bridged thiolate sulfur S(1); i.e., P(2) is in the basal position of the pseudo square pyramid. Both CO groups at the Fe(1) centers are *trans* to bridged thiolates. The structure of **[(μ-H)-anti-2$^+$]** differs only from **anti-2** in that the bridging hydride takes the position of the Fe−Fe bond density. The more symmetrical **syn-2**, Figure 3, positions both P-donor sites *cis* to the Fe−Fe bond and *trans* to the bridged thiolates. Two phenyl groups are below the Fe−Fe bond vector.

Metric parameters for the butterfly Fe_2S_2 core structures are substantially the same for all with acute $\angle$Fe−S−Fe's, and as shown in Figure 5, the three structures closely overlay in that core (rms deviation of 6.4%). The dihedral angle defined by the intersections of S(1)Fe(1)Fe(2) and S(2)Fe-

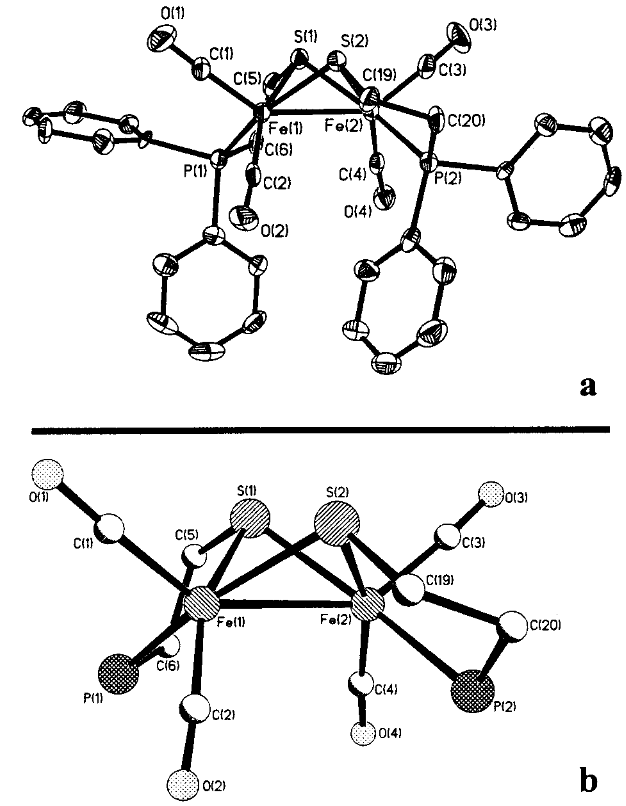

Figure 3. (a) Thermal ellipsoid (50%) and (b) ball-and-stick representations of the molecular structure of **syn-2**.

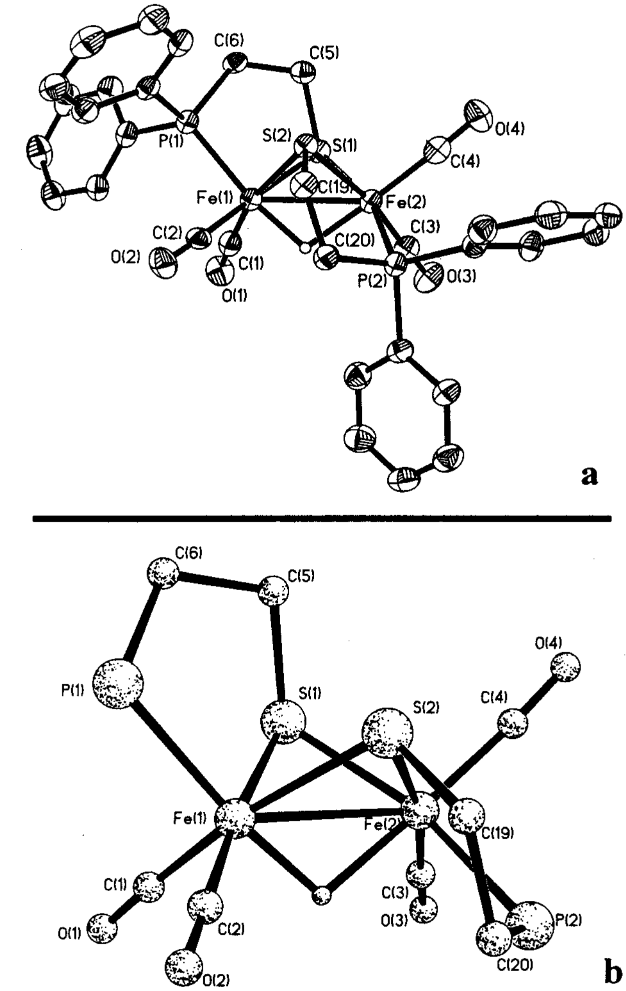

Figure 4. (a) Thermal ellipsoid (50%) and (b) ball-and-stick representations of the molecular structure of **[(*μ*-H)-anti-2]$^+$**.

(1)Fe(2) planes is 99.3° in **syn-2** and is slightly smaller than that of **anti-2**, 104.5°, and of **[(*μ*-H)-anti-2]$^+$**, 105.6°. Consistently, the distances between two thiolate sulfur "wing tips" are 2.826 Å for **syn-2** and 2.945 Å for **anti-2**. The analogous distance in the **[(*μ*-H)-anti-2]$^+$** structure is 2.969 Å.

The Fe−P and Fe−C bond distances displayed in Table 2 for **anti-2** are typical in comparison to monodentate analogues $[Fe(CO)_2L(\mu\text{-SR})]_2$ (L = $P(CH_3)_3$, R = CH_3).[7] There are no significant differences in lengths of the Fe−CO bond *trans* to the bridged thiolate ligand and the Fe−CO *trans* to the metal−metal bond. The average Fe−S and Fe−P bond distances, 2.265(2) and 2.209(3) Å, respectively, of the **syn-2** isomer are not distinguishable from those of the **anti-2**. This indicates that the disposition of the pendant ethylene groups has no significant effect on the Fe_2S_2 core, consistent with the similarity in ν(CO) IR pattern, *vide infra*. The Fe−Fe bond distance of 2.604(2) Å is slightly longer for **syn-2** than that found in **anti-2**, 2.562(1) Å, while the Fe−Fe distance of the **[*μ*-H-anti-2]$^+$**, 2.580(1) Å, shows little effect of protonation. Other selected bond distances and angles for **syn-2** are shown in Table 3.

The asymmetry in the P-donor positions of **anti-2** produces an asymmetric bridging hydride ligand; the bond distance of that *trans* to the phosphine, Fe(1)−H(1), is 1.59(1) Å while that *trans* to the CO, Fe(2)−H(1), is 1.74(1) Å. Although the incorporation of hydride, with concomitant oxidation of the Fe^IFe^I to $Fe^{II}Fe^{II}$, produces no structural changes in the Fe_2S_2 core, electrochemical and spectral properties show considerable differences.

Table 2. Selected Bond Distances (Å) and Angles (deg) for *anti*-(μ-$SCH_2CH_2PPh_2)_2Fe_2(CO)_4$, **anti-2**, and ($\mu$-H)-*anti*-($\mu$-$SCH_2CH_2PPh_2)_2Fe_2(CO)_4{}^+$, **[(*μ*-H)-anti-2]$^+$**

	anti-2	**[(*μ*-H)-anti-2]$^+$**
Fe(1)−Fe(2)	2.562(1)	2.580(10)
Fe(1)−P(1)	2.216(1)	2.2360(14)
Fe(2)−P(2)	2.214(1)	2.2235(13)
Fe(1)−S(1)	2.264(1)	2.2671(13)
Fe(2)−S(2)	2.223(1)	2.2470(13)
Fe(2)−S(1)	2.271(1)	2.2665(13)
Fe(1)−S(2)	2.275(1)	2.2851(13)
Fe(2)−C(4)	1.777(2)	1.787(5)
Fe(2)−C(3)	1.769(2)	1.797(5)
Fe(1)−C(1)	1.766(3)	1.790(5)
Fe(1)−C(2)	1.743(3)	1.789(5)
Fe(1)−H		1.587(6)
Fe(2)−H		1.740(6)
S(1)Fe(1)S(2)	80.9(1)	81.42(5)
S(1)Fe(2)S(2)	81.9(1)	82.27(5)
Fe(1)S(1)Fe(2)	68.8(1)	69.37(4)
Fe(1)S(2)Fe(2)	69.4(1)	69.39(4)
P(1)Fe(1)C(1)	107.6(1)	95.10(15)
P(1)Fe(1)C(2)	98.8(1)	98.37(15)
P(1)Fe(1)S(1)	88.4(1)	87.15(5)
P(1)Fe(1)S(2)	92.1(1)	92.45(5)
C(4)Fe(2)P(2)	95.1(1)	98.09(15)
C(4)Fe(2)C(3)	99.8(1)	93.9(2)
P(2)Fe(2)S(2)	87.1(1)	87.84(5)

Electrochemistry. Electrochemical studies were performed on mixtures of *anti* and *syn* compounds in acetonitrile solutions; however, the separated, pure isomers showed very similar electrochemical behavior. As shown in Figure 6, the

Table 3. Selected Distances (Å) and Angles (deg) for *syn*-(μ-$SCH_2CH_2PPh_2$)$_2$$Fe_2(CO)_4$, **syn-2**[a]

Fe(1)−Fe(2)	2.603(2)		
Fe(2)−S(1)	2.265(2)	Fe(2)−S(2)	2.269(2)
Fe(1)−S(1)	2.250(2)	Fe(1)−S(2)	2.277(2)
Fe(2)−P(2)	2.207(2)	Fe(1)−P(1)	2.211(2)
Fe(2)−C(3)	1.785(9)	Fe(2)−C(4)	1.753(8)
Fe(1)−C(1)	1.780(8)	Fe(1)−C(2)	1.753(8)
C(1)−O(1)	1.147(9)	C(2)−O(2)	1.159(9)
C(3)−O(3)	1.150(9)	C(4)−O(4)	1.179(9)
S(1)−Fe(1)−S(2)	77.26(8)	S(1)−Fe(2)−S(2)	77.10(8)
Fe(1)−S(1)−Fe(2)	70.43(7)	Fe(1)−S(2)−Fe(2)	69.87(7)
S(1)−Fe(1)−P(1)	86.78(9)	S(2)−Fe(2)−P(2)	86.72(8)
S(2)−Fe(1)−P(1)	159.54(9)	S(1)−Fe(2)−P(2)	162.21(9)
C(1)−Fe(1)−P(1)	101.2(3)	C(1)−Fe(1)−S(1)	103.4(3)
C(3)−Fe(2)−P(2)	95.6(3)	C(3)−Fe(2)−S(2)	103.2(3)
C(1)−Fe(1)−C(2)	97.9(3)	C(3)−Fe(2)−C(4)	97.9(4)

[a] Estimated standard deviations are given in parentheses.

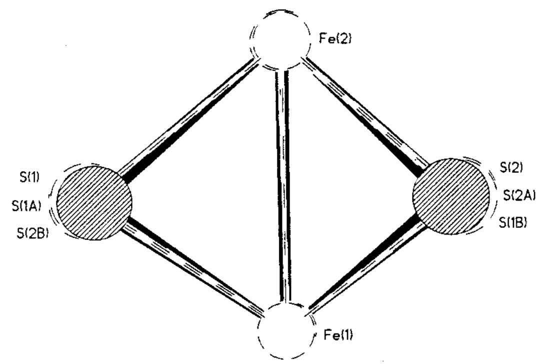

Figure 5. Overlay of the Fe_2S_2 cores of **anti-2**, **syn-2**, and **[(μ-H)-anti-2]$^+$**.

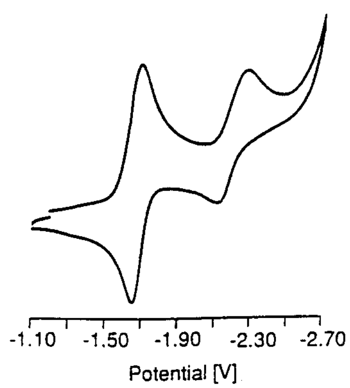

Figure 6. Cyclic voltammogram of 5 mM solution (μ-$SCH_2CH_2PPh_2$)$_2$-$Fe_2(CO)_4$ in 0.1 M [(n-Bu)$_4$N][PF_6]/CH_3CN with a glassy carbon working electrode at a scan rate of 200 mV/s.

cyclic voltammogram of (μ-$SCH_2CH_2PPh_2$)$_2$$Fe_2(CO)_4$ in CH_3-CN (as a mixture of isomers) shows two features at potentials between −1.5 and −3.0 V. One quasi-reversible wave is centered at −1.67 V (ΔE_p = 0.60 V) and is assigned to a one-electron reduction at an iron atom to give the $[Fe^IFe^0]^-$ or (μ-$SCH_2CH_2PPh_2$)$_2$$Fe_2(CO)_4^-$ (radical anion). A quasi-reversible wave centered at −2.20 V is assigned to a second electron reduction, presumed to have an $[Fe^0Fe^0]$ center in the dianion or (μ-$SCH_2CH_2PPh_2$)$_2$$Fe_2(CO)_4^{2-}$. The formation of the radical anion and dianionic species is also confirmed by chemical reduction (*vide infra*). The finding of two one-electron reductions for (μ-$SCH_2CH_2PPh_2$)$_2$$Fe_2(CO)_4$ contrasts to the one two-electron step reported for the phosphido-bridged diiron carbonyl compound, $[Fe(CO)_3(PPh_2)]_2$ (−1.2 V vs SCE, ΔE_p = 45 mv).[22] In addition, an irreversible feature observed at +0.33 V is assumed to be S-based.

The cyclic voltammogram of (μ-H)(μ-$SCH_2CH_2PPh_2$)$_2$)-$Fe_2(CO)_4^+(SO_3CF_3)^-$ has two irreversible redox processes at −0.60 and −0.90 V, assigned to reductions to $Fe^{II}Fe^I$ and Fe^IFe^I species. Repetitive scanning resulted in the buildup of waves at −1.71 and −2.28 V, consistent with the formation of the neutral (μ-$SCH_2CH_2PPh_2$)$_2$$Fe_2(CO)_4$ parent compound. This was confirmed by bulk chemical reduction of the cationic hydride.

Chemical Reduction. On bulk chemical reduction of neutral (μ-$SCH_2CH_2PPh_2$)$_2$$Fe_2(CO)_4$ with excess Na/Hg amalgam in CH_3CN under argon for about 1 h, the CO stretching frequencies at 1989 (m), 1952 (s), and 1909 (m, br) were observed to shift to 1956 (s), 1896, (s, br), and 1732 (m) cm^{-1}, Figure 1f. A UV−vis spectral monitor of the reaction also shows a decrease in the absorbance at 360 nm. The first reduction species, **3**, was isolated as a dark red-brown solid with PPN^+ as counterion. This solid is highly air sensitive even in the solid state and returns to the starting material, neutral (μ-$SCH_2CH_2PPh_2$)$_2$$Fe_2(CO)_4$, on exposure to O_2. The IR spectrum, Figure 1f, is interpreted as an Fe^0-Fe^I dimer with a bridging CO group between the two iron centers as proposed herein, complex **3**. In support of this

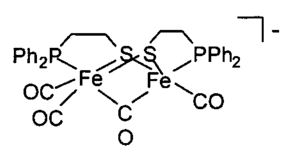

3

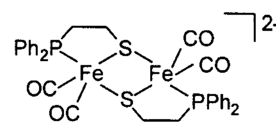

4

assignment, we note that the reported anionic species, [(μ-SEt)(μ-CO)$Fe_2(CO)_6$]$^-$,[23] and [(μ-PPh_2)(μ-CO)$Fe_2(CO)_5$-(PPh_2H)]$^-$,[24] displayed bridging CO frequencies at 1743 and 1710 cm^{-1}, respectively. The spectral properties of an intermediate in the CN^-/CO substitution reaction of an Fe^I-Fe^I dimer rendered unsymmetric due to a thioether on one iron was also interpreted as having a bridging CO of ν(CO) = 1780 cm^{-1}.[25]

On continuation of the reduction of (μ-$SCH_2CH_2PPh_2$)$_2$-$Fe_2(CO)_4$ by Na/Hg in CH_3CN overnight under argon, two new peaks in the CO stretching region grew in at 1941 (s) and 1854 (s) cm^{-1}, reaching a maximum intensity after several days. This *extremely* air-sensitive compound **4** is tentatively formulated as a dianionic Fe^0Fe^0 species as described above in the electrochemistry results. Notably, these reaction conditions do not reliably yield pure **4**, but rather often a mixture of **4** and the parent, neutral (μ-SCH_2-CH_2PPh_2)$_2$$Fe_2(CO)_4$, **2**. Since **2** readily forms on exposure

(21) De Beer, J. A.; Haines, R. J. *J. Organomet. Chem.* **1972**, *36*, 297.
(22) Collman, J. P.; Rothrock, R. K.; Finke, R. G.; Moore, E. J.; Rose-Munch, F. *Inorg. Chem.* **1982**, *21*, 146.
(23) Seyferth, D.; Womack, G. B.; Dewan, J. C. *Organometallics* **1985**, *4*, 398.
(24) Yu, Y.-F.; Gallucci, J.; Wojcicki, A. *J. Am. Chem. Soc.* **1983**, *105*, 4826.
(25) Razavet, M.; Davies, S. C.; Hughes, D. L.; Pickett, C. J. *Chem. Commun.* **2001**, 847.

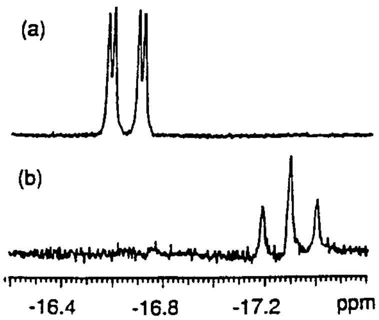

Figure 7. ^{1}H NMR spectrum in upfield region for (a) **[(μ-H)-anti-2]**$^+$[SO_3CF_3]$^-$; and (b) **[(μ-H)-syn-2]**$^+$[SO_3CF_3]$^-$ in d_6-acetone.

of compounds **3** and **4** to air or to protonic acids, we assume that its formation after long reaction times results from adventitious acid or O_2.

Solution Spectral Properties of the Bridging Hydrides and Deprotonation Reactions. Both **anti-2** and **syn-2** react with a slight excess of CF_3SO_3H in THF solution, yielding orange-red solutions whose ν(CO) infrared spectra displayed three bands approximately 60 cm^{-1} higher in energy than those of their neutral (μ-$SCH_2CH_2PPh_2$)$_2Fe_2(CO)_4$ precursors, Table 1. As shown in Figure 1, traces d and e, the CN_3CN solution ν(CO) infrared spectra of the cationic hydrides show greater distinctions between the isomeric forms than those between the neutral parent precursors. The **[(μ-H)-anti-2]**$^+$ spectrum is resolved into four peaks while that of **[(μ-H)-syn-2]**$^+$ shows only two, positioned at the average of the higher and the two lower bands of the *anti* isomer.

The ^{1}H NMR spectrum (Figure 7a) of **[(μ-H)-anti-2]**$^+$[SO_3CF_3]$^-$ showed a doublet of doublets in the upfield region, centered at δ −16.85 with coupling constants of J_{P-H} = 23.8 and 4.8 Hz. In addition, the downfield resonance region also shows two different sets of ethylene protons for the ligand. The ^{31}P NMR shows doublets at δ 88.1 and 79.1 ppm each with J_{P-P} = 11 Hz. This spectroscopic data is consistent with the molecular structure of **[(μ-H)-anti-2]**$^+$, as described above and presented in Figure 4; i.e., the bridged hydride is coupled to two nonequivalent phosphorus atoms from nonequivalent P to S ethylene linkers.

The ^{1}H NMR spectrum for the product resulting from protonation of **syn-2**, Figure 7 b, has an upfield triplet centered at δ −17.4 ppm which integrates as one proton compared to 28 in the ligand resonance region. The triplet, J_{P-H} = 21.0 Hz, results from equal coupling of the bridged hydride and the two P atoms of the syn isomer. The compound **[(μ-H)-syn-2]**$^+$[SO_3CF_3]$^-$ is more thermally stable than **[(μ-H)-anti-2]**$^+$[SO_3CF_3]$^-$. Notably, the ^{1}H NMR spectrum obtained on the product of protonation of the mixture of **syn-2** and **anti-2** as isolated in the original synthesis, eq 3, showed a mixture of **[(μ-H)-anti-2]**$^+$ and **[(μ-H)-syn-2]**$^+$ isomers, stable in the dark, but undergoing isomerization and increasing the **[(μ-H)-syn-2]**$^+$ in the light. Interestingly, the presence of NEt_3 promotes isomerization of **[(μ-H)-anti-2]**$^+$ to **[(μ-H)-syn-2]**$^+$, *vide infra*.

An analogous (μ-H)[Fe(CO)$_2$(PMe$_2$Ph)(μ-SMe)]$_2^+$ complex, with δ = −16.6 ppm (triplet, J_{P-H} = 4.4 Hz), was reported to result from protonation of [Fe(CO)$_2$(PMe$_2$Ph)(μ-SMe)]$_2$ with various acids.[26,27] In this case only one bridged hydride species, i.e., the *syn* isomer with both PMe$_2$Ph ligands in apical (or *trans* to the μ-H) positions, was reported. From this work and ours we can conclude that the absolute value of the J_{P-H} of P *trans* to the μ-H in **[(μ-H)-anti-2]**$^+$ is smaller than *cis* coupling.

The bridged hydride cations were readily (on time of mixing) deprotonated by equimolar amounts of $NEt_4^+CN^-$ in CH_3CN, regaining the neutral parent complexes. Acetonitrile solutions of bistriphenylphosphineimminium chloride, PPN$^+$Cl$^-$, also rapidly reacted; however, a 5-fold excess of chloride resulted in only partial deprotonation. Equilibrium was established more rapidly for the **[(μ-H)-anti-2]**$^+$ isomer. In contrast, 5, 10, and 20 equiv of the strong but neutral base, triethylamine, required hours to achieve equilibrium with **[(μ-H)-syn-2]**$^+$ as its triflate salt in THF. Qualitative differences in rates suggest more rapid deprotonation reactions of Et_3N with **[(μ-H)-anti-2]**$^+$[SO_3CF_3]$^-$, consistent with less steric hindrance in this isomer as compared to **[(μ-H)-syn-2]**$^+$ where the bridging hydride is sterically protected by two flanking phenyl groups. Such a steric argument is appealing in that for the **[(μ-H)-anti-2]**$^+$ the bridged hydride is *trans* to the better σ-donor ligand phosphine which should, relative to **[(μ-H)-syn-2]**$^+$, inhibit removal of hydrogen as a proton should electronic factors predominate. Addition of small (ca. 10%) amounts of PPN$^+$Cl$^-$ facilitated rates of deprotonation by NEt_3.

It should be mentioned that deprotonation of **[(μ-H)-anti-2]**$^+$[SO_3CF_3]$^-$ by NEt_3 is complicated by an isomerization process, as yet not clarified. On addition of a stoichiometric amount of NEt_3 to solutions containing only **[(μ-H)-anti-2]**$^+$[SO_3CF_3]$^-$, the triplet characteristic of the *syn* isomer **[(μ-H)-syn-2]**$^+$ grew in while the doublet of doublets for the **[(μ-H)-anti-2]**$^+$ diminished in intensity and broadened. It is not clear whether the broadening is due to exchange of the proton of **[(μ-H)-anti-2]**$^+$ with $HNEt_3^+$ or to quadrupolar broadening from interaction of the metal-bound proton with NEt_3. In either case, we can assume that the observation signifies similar basicities of NEt_3 and the Fe−Fe bond density of neutral binuclear **anti-2**. This effect was not observed with the poorer base pyridine. The ability of NEt_3 to partially remove a proton from metal carbonyl hydrides such as HCo(CO)$_4$, producing a Co$^-$- - -H$^+$- -NEt_3 tight ion pair (alternately represented as a metal−H-bonded species), has been established.[28,29] Likewise well-known are the effects of steric blocks on the rates of deprotonation of metal hydrides in [HMo(CO)$_2$(diphos)$_2$]$^+$, as well as the proton-carrying effect of hard bases such as chloride.[30−32]

(26) Fauvel, K.; Mathieu, R.; Poilblanc, R. *Inorg. Chem.* **1976**, *15*, 976.
(27) Savariault, J.-M.; Bonnet, J.-J.; Mathieu, R.; Galy, J. *C. R. Acad. Sci. Paris, t.* **1977**, 284.
(28) Calderazzo, F.; Fachinetti, G.; Marchetti, F.; Zanazzi, P. F. *J. Chem. Soc., Chem. Commun.* **1981**, 181.
(29) Mareque Rivas, J. C.; Brammer, L. *Coord. Chem. Rev.* **1999**, *183*, 43.
(30) Darensbourg, M. Y.; Ludvig, M. M. *Inorg. Chem.* **1986**, *25*, 2894.
(31) Liu, W.; Thorp, H. H. *J. Am. Chem. Soc.* **1995**, *117*, 9822.
(32) Kristjánsdottir, S. S.; Norton, J. K. In *Transition Metal Hydride*; Dedieu, A., Ed.; VCH: New York, 1992; pp 309−359.

Scheme 4

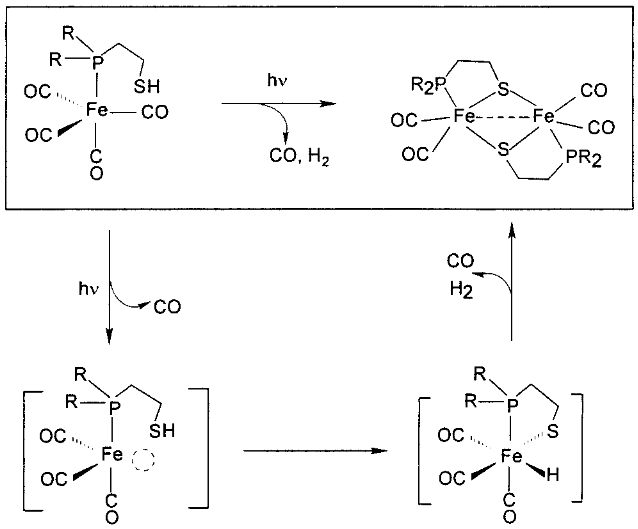

Effects of P-Donor Strengths in $PPh(CH_3)CH_2CH_2SH$ and $P(CH_3)_2CH_2CH_2SH$ Derivatives. Under photochemical experimental conditions as similar as possible it was established that, relative to complex **1**, $Fe(CO)_4(PPh_2CH_2CH_2SH)$, extended periods of irradiation of THF solutions of $Fe(CO)_4(PPhMeCH_2CH_2SH)$ were required to produce the dinuclear iron dicarbonylphosphino-thiolate analogue of complex **2**. Extended irradiation of solutions of $Fe(CO)_4(PMe_2CH_2CH_2SH)$ under similar photolytic conditions caused no reaction as indicated by the infrared spectral monitor.

Discussion

Reaction Pathway. Although the overall reaction pathway for the synthesis of binuclear phosphino thiolates from thiols is still uncertain, Scheme 4 expresses the most obvious features as highlighted in our work. A coordinately unsaturated $Fe(CO)_4$ fragment is preferentially captured by the phosphine donor atom in the P-SH ligand (rather than the thiol sulfur donor), and the 18-electron mononuclear Fe(0) complex serves as precursor to the binuclear product. Photolysis is required to eject CO and provide a second open site which we propose is required for the binding and activation of the tethered thiol. Yet another CO must be lost, along with intermolecular generation of H_2, in order to complete the reaction.[4] The different requirements of UV irradiation times for the three phosphino thiols relate to the electronic differences in the P-donor ligand consistent with better donors inhibiting CO loss.

An alternative mechanism involving initial RSH binding S−H oxidative addition, producing a binuclear intermediate with bridging thiolates and dangling phosphines, is not indicated as all three phosphinothiols should have produced binuclear Fe_2S_2 products. In fact, the superior ligating ability of phosphine over thiols was illustrated in the isolation of the series, $Fe(CO)_4(PMe_2CH_2CH_2SH)$, $Fe(CO)_4(PPhMeCH_2CH_2SH)$, and $Fe(CO)_4(PPh_2CH_2CH_2SH)$. Should protonation or oxidative addition of the thiol proton to the 18-electron Fe(0) complex (without CO loss and binding of the thiolate) govern the reaction pathway, the complex containing the best electron-donor ligand, the $Fe(CO)_4(PMe_2CH_2CH_2SH)$ complex, should be preferentially protonated. The trend in reactivity is, however, opposite and is taken as evidence of the predominating influence of Fe−CO bond lability from the Fe^0 parent complex on the reaction progress. Note that the mechanism in Scheme 4 does not indicate possible binucleating steps which might occur as follows: Increased CO lability is expected for the Fe^{II} thiolate hydride which would open a site for the first thiolate bridge formation. A possibility is shown in the arrangement below whereby thiol binding to one Fe^0 results in increased acidity and protonation of a second Fe^0 generating a thiolate-bridged Fe^{II} hydride. Subsequent protonation of the hydride by the dangling thiol must be followed by several steps, including H_2 loss, CO loss, a second thiolate bridge formation and $Fe^{II}Fe^0$ comproportionation to Fe^IFe^I. Precedents for such intramolecular H^+/H^- reactivity in simpler mononuclear complex chemistry include the protonation of a Ru−H by an amine−H^+, tethered to η^5-C_5H_4R.[33−35]

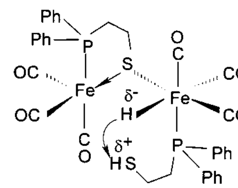

Structures. Three features relating to the X-ray crystal structures are considered most important:

(1) *The orientation of the α-C on the bridging thiolates dictates the position of phosphorus atoms on each iron.* The differences in *syn*, *anti*, and *syn′* S−C arrangements in all CO dinuclear iron complexes with monodentate μ-SR bridges are of little consequence to electronic effects from the bridging sulfur donor. However, in the case of dinuclear complexes containing bidentate S−P complexes, the subsequent positioning of the P-donor ligand as a result of directionality of the S−C_α position produces isomers with the metal−metal bond density or μ-H in different electronic environments dependent on whether the P-donor is *cis* or *trans* to that position.

(2) The molecular structures of three binuclear complexes show *insignificant differences in Fe−Fe distances despite the fact that in the Fe^IFe^I complexes there is a formal metal−metal bond whereas in the $Fe^{II}(\mu$-H)Fe^{II} complex there is none.* Other Fe−L distances and the Fe_2S_2 cores are also the same. The Fe−Fe bond density therefore presents a site in which a proton might be taken up and stored as a hydride without impacting the overall structure of the binuclear complex.

(3) This study provides another example of the *interesting similarities of dinuclear Fe^IFe^I complexes with the active site of Fe-only hydrogenase in terms of the Fe_2S_2 core.* It indicates that the Fe−Fe distances of 2.60 Å in the binuclear

(33) Ayllon, J. A.; Sayers, S. F.; Sabo-Etienne, S.; Donnadieu, B.; Chaudret, B. *Organometallics* **1999**, *18*, 3981.
(34) Caballero, A.; Jalón, F. A.; Manzano, B. R. *Chem. Commun*. **1998**, 1879.
(35) Chu, H. S.; Lau, C. P.; Wong, K. Y. *Organometallics* **1998**, *17*, 2768.

active site of Fe-only hydrogenases[14] can be consistent with an Fe–Fe bond and $Fe^{I}Fe^{I}$ oxidation states as well as a face-bridged bioctahedron in $Fe^{II}(\mu\text{-H})Fe^{II}$ complexes.[36]

The Bridging Hydride as a Proton. The basicity of M–M bonds is sensitive both to the M and to substituent ligands. Whereas (μ-pdt)$Fe_2(CO)_6$ cannot be protonated, the (μ-pdt)$Fe_2(CO)_4(PMe_3)_2$ readily forms a stable bridging hydride complex.[37] Likewise Nataro and Angelici have shown the PMe_3 derivative of $Cp_2Mo_2(CO)_4(PR_3)_2$ to be "dramatically" more basic than its PMe_2Ph analogue.[38]

Perhaps the most extraordinary result of our study is the ease with which the bridging hydride can be extracted as a proton from the Fe–Fe bond density by anionic bases, even the very weak base, chloride. Thermodynamic driving forces include the formation of beneficial ion pairs in the low-polarity solvents which were used, as well as the reclamation of the Fe–Fe bond density. Contributors to the kinetic barrier include polarization of the electron density surrounding the hydride which, *a priori*, might have been considered significant in a binuclear bridging hydride, Scheme 5. On the other hand, the electronic rearrangement is shared between two metals and, as noted by the crystal structures, exacts a minimal structural change. In this manner of electron density delocalization, the enhanced acidity of bridging hydrides in polynuclear complexes has previously been described for $H_4Os_4(CO)_{12}$.[39,40] The efficacy of binuclear active sites with M···M distances within bonding range in enzyme catalysis could lie in such a dispersal of electronic changes as proton/electron coupled reactions take place.

Scheme 5

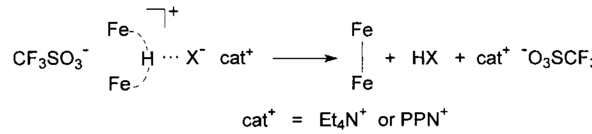

Acknowledgment. We acknowledge financial support from the National Science Foundation (CHE 98-12355 for this work, CHE 85-13273 for the X-ray diffractometer and crystallographic computing system) and contributions from the R. A. Welch Foundation. Appreciation is expressed to Matthew L. Miller for technical assistance with molecular structure displays as well as to Susan Winters for manuscript preparation.

Supporting Information Available: X-ray crystallographic tables for *anti*-(μ-$SCH_2CH_2PPh_2$)$_2Fe_2(CO)_4$, *syn*-(μ-$SCH_2CH_2PPh_2$)$_2$-$Fe_2(CO)_4$, and **[(μ-H)-anti-2]**$^+[SO_3CF_3]^-$. Crystallographic data in CIF format. This material is available free of charge via the Internet at http://pubs.acs.org.

IC010741G

(36) De Lacey, A. L.; Stadler, C.; Cavazza, C.; Hatchikian, E. C.; Fernandez, V. M. *J. Am. Chem. Soc.* **2000**, *122*, 11232.
(37) Zhao, X.; Georgakaki, I. P.; Miller, M. L.; Yarbrough, J. C.; Darensbourg, M. Y. *J. Am. Chem. Soc.* **2001**, *123*, 9710.
(38) Nataro, C.; Angelici, R. J. *Inorg. Chem.* **1998**, *37*, 2975.
(39) Kristijánsdóttir, S. S.; Moody, A. E.; Weberg, R. T.; Norton, J. R. *Organometallics* **1988**, *7*, 1983.
(40) Walker, H. W.; Pearson, R. G.; Ford, P. C. *J. Am. Chem. Soc.* **1983**, *105*, 1179.